# Effective functional form of Regge trajectories

M. M. Brisudová,* L. Burakovsky,† and T. Goldman‡

*Theoretical Division, MS B283, Los Alamos National Laboratory, Los Alamos, New Mexico 87545*

We present theoretical arguments and strong phenomenological evidence that hadronic Regge trajectories are essentially nonlinear and can be well approximated, for phenomenological purposes, by a specific square-root form.

PACS number(s): 12.40.Nn, 12.39.Ki, 12.40.Yx

## I. INTRODUCTION

It is well known that the hadrons composed of light $[n \equiv (u,d),s]$ quarks populate approximately linear Regge trajectories; i.e., the orbital momentum $l$ of the state is proportional to its mass: $l = \alpha' M^2(l) + \alpha(0)$, where the slope $\alpha'$ depends weakly on the flavor content of the states lying on the corresponding trajectory. Therefore, knowledge of Regge slopes and intercepts is very useful for spectral purposes. Since knowledge of Regge trajectories in the scattering region $(t < 0)$ is also useful for many nonspectral purposes, e.g., in the recombination and fragmentation models, Regge trajectories become a valuable description of hadron dynamics, perhaps generally more important than the mass of any particular state.

In the Veneziano model for scattering amplitudes [1] there are infinitely many excitations populating linear Regge trajectories. The same picture of linear trajectories arises from a linear confining potential [2] and the string model of hadrons [3].

However, the realistic Regge trajectories extracted from data are *nonlinear*. Indeed, the straight line which crosses the $\rho$ and $\rho_3$ squared masses corresponds to an intercept $\alpha_\rho(0) = 0.48$, whereas the physical intercept is located at 0.55, as discussed below. The nucleon Regge trajectory, as extracted from the $\pi^+ p$ backward scattering data, is [4]

$$\alpha_N(t) = -0.4 + 0.9t + \tfrac{1}{2} 0.25 t^2, \tag{1}$$

and contains positive curvature. Recent UA8 analysis of the inclusive differential cross sections for the single-diffractive reactions $p\bar{p} \to pX$, $p\bar{p} \to X\bar{p}$ at $\sqrt{s} = 630$ GeV reveals a similar curvature of the Pomeron trajectory [5]:

$$\alpha_P(t) = 1.10 + 0.25t + \tfrac{1}{2}(0.16 \pm 0.02)t^2. \tag{2}$$

An essentially nonlinear $a_2$ trajectory was extracted in Ref. [6] for the process $\pi^- p \to \eta n$.

In addition to being disfavored by these experiments, linear trajectories also lead to problems in theory. Linear trajectories violate the Cerulus-Martin fixed angle scattering bound [7]. (The so-called ''square-root'' trajectory, used ex-

tensively in this paper for spectroscopic purposes, saturates this bound [8].) Further, they violate the Froissart bound, in the following sense: The consequences of the strong duality between the saturation of the $S$-matrix by (i) narrow resonances [9] and (ii) Regge asymptotic behavior [10] in the $S$-matrix formulation of statistical mechanics by Dashen, Ma and Bernstein [11] were studied in [12]. There it was shown that in order that the total cross section satisfy the Froissart bound [13], $\sigma_{tot}(s) \leqslant A \ln^2 s$, $A = \text{const}$, the density of resonances in the elastic amplitude should decrease with energy, typically as $\sim 1/E$ [12]. [A decreasing density of resonances is a typical feature of dual amplitudes with Mandelstam analyticity (DAMA) [14].] A linear trajectory violates the requirement of a decreasing density of resonances (for a linear trajectory, the density of resonances grows as $\sim E^3$ [15]), and therefore, violates the Froissart bound in this framework.

Linear trajectories arose in the context of the string model of hadrons. Modern approaches to string field theory may be able to resolve such inconsistency problems with unitarity [16]. It might be conjectured, therefore, that their hadronic trajectories are not linear, either. Unfortunately, at present there is still a large gap between fundamental string theories and hadron phenomenology. However, we wish to emphasize that we do not invoke fundamental string field theory in our arguments below. We refer to a classical string theory as a convenient mathematical tool for the representation of physical string-like objects, such as flux tubes, with the heuristic inclusion of color-screening effects.

The idea of nonlinear Regge trajectories is not new. In the late 1960s, by introducing Regge cuts through the eikonal method, a number of authors have shown that the effective trajectory for large momentum transfer $(-t)$ goes like $\sqrt{-t}$ [17]. Subsequent comprehensive analysis by Vasavada, combining both Regge poles and cuts, arrived at the effective square-root trajectory in the entire complex angular-momentum plane [18]. The $\alpha(t) \sim \sqrt{-t}$ trajectory was also found by Gribov *et al.* [19] in a Pomeron-Reggeon field theory. Other nonlinear forms have been also studied in the literature.

Once the nonlinearity of Regge trajectories is an established fact, the determination of its actual form becomes an important issue. The main prupose of this paper is to argue, from both theory and phenomenology, that hadronic Regge trajectories are nonlinear and terminate. We start in Sec. II with a model study of a heavy quark-antiquark system in a potential fitted to the results of an unquenched lattice QCD [20], and show that its (parent) Regge trajectory is equally

*Email address: brisuda@t5.lanl.gov
†Email address: burakov@t5.lanl.gov
‡Email address: goldman@t5.lanl.gov

well fitted by both limiting cases of nonlinear forms allowed by dual amplitudes with Mandelstam analyticity (DAMA) [21]. (Thus, one can argue that all these nonlinear forms would fit the trajectory as well. The two limiting cases are the so-called ''square-root'' trajectory and the ''logarithmic'' trajectory.) To gain some understanding of this peculiar observation, we turn to an analytic model which allows us to recover an underlying potential from a known Regge trajectory. It is a model of a classical massless string with a variable tension (Sec. III). Such a string might be a representation of a color-screened flux tube. (We show that this model is a relativistic generalization of a nonrelativistic rod with arbitrary potential, in the same sense as the usual Nambu-Goto string model is a generalization of a nonrelativistic linear potential model.) We present the two potentials corresponding to the square-root and logarithmic trajectories, respectively, and compare them with the unquenched lattice QCD potential [22] used in the heavy quark model. The two models (Sec. II vs Sec. III) are very different, but since the nonlinearity of Regge trajectories arises due to the flux tube breaking [20], one can expect the same *qualitative* behavior in both heavy and light quark systems.

Sections II and III show that even though the two extreme nonlinear forms can both fit the bound states spectra, one of them, the square-root form, goes beyond the position of the few lowest lying poles. This is why we choose the square-root form to fit and predict real-world spectra in Sec. IV. It should be noted that any nonlinear form bracketed by the square-root and logarithmic ones can be expected to give comparably good results for the lowest lying states, and a true test would be higher excited states (likely not yet observed).

With a few additional assumptions that are commented on as they are introduced, we obtain an excellent agreement with data. This means that the Regge trajectories are indeed nonlinear, and well approximated by the square-root form. We summarize and comment on some of the results at the end of Sec. IV. The last section contains our overall summary and conclusions.

## II. HEAVY QUARKONIA MODEL

In a previous paper [20] we considered a Hamiltonian model for heavy quarks which attempted to include the effect of light pair creation, or, in other words, the breaking of the flux tube stretched between the two heavy sources that inevitably occurs when the distance between the sources is sufficiently large. We have shown that consequently, Regge trajectories for the heavy quarkonia become nonlinear and their real parts terminate. In this paper we use the model to gain insight about the specifics of the (nonlinear) form of hadronic Regge trajectories.

A meson consisting of two heavy quarks is well described in leading order by a nonrelativistic, spin-independent Hamiltonian, viz.

$$H = -\frac{1}{2m}\mathbf{\nabla}^2 + V(r), \qquad (3)$$

where $m = M/2$ is the reduced mass, with $M = 5.2$ GeV, and $V(r)$ denotes a potential. We use $M = 5.2$ GeV, and a potential fit to results of unquenched lattice QCD calculation for infinitely heavy sources. We have argued that our simple two body calculation produces results qualitatively similar to coupled channel method, because it dynamically takes into account coupling to open channels, and that the two approaches can be expected to differ significantly only for a few states near the threshold [20].

The screened static potential fitted to results of lattice calculations is [22]

$$V(r) = \left(-\frac{\alpha}{r} + \sigma r\right)\frac{1 - e^{-\mu r}}{\mu r}, \qquad (4)$$

where $\mu^{-1} = (0.9 \pm 0.2)$ fm $= (4.56 \pm 1.01)$ GeV$^{-1}$, $\sqrt{\sigma} = 400$ MeV and $\alpha = 0.21 \pm 0.01$. We obtain bottomonium-like spectra by diagonalizing the Hamiltonian (3) with the potential (4). The number of bound states in the model is finite, and it decreases with increased screening $\mu$. The number of bound states is the largest for the parent trajectory, and decreases by one unit for each consecutive daughter. Another important feature of the Regge trajectories in this model is that they acquire curvature due to screening of the linear potential. Since we are interested in how the screening affects the form of the Regge trajectories (which would be linear in the absence of screening), for maximum reliability of the numerical fits it is useful to consider the case of a Regge trajectory with the largest number of bound states. Therefore, in what follows we concentrate on the parent trajectory for $\mu^{-1} = 0.9$ fm $= 0.18$ GeV$^{-1}$. The same conclusions as those presented below hold for all $\mu$ in the range indicated by the fit to the lattice data [22].

A meson trajectory $\alpha_{j\bar{i}}(t)$, can be parametrized on the whole physical sheet in the following form:

$$\alpha_{j\bar{i}}(t) = \alpha_{j\bar{i}}(0) + \gamma[T_{j\bar{i}}^\nu - (T_{j\bar{i}} - t)^\nu], \qquad 0 \leq \nu \leq \frac{1}{2}. \quad (5)$$

(up to a power of logarithm), assuming that $\alpha_{j\bar{i}}(t)$ is an analytic function having a physical cut from $t_0$ to $\infty$, it is polynomially bounded on the whole physical sheet, and there exists a finite limit of the trajectory phase as $|t| \to \infty$ [23]. Here[1] $\gamma$ is the universal slope which nonlinear trajectories must have in asymptopia [24],

$$\alpha(t) \sim -\gamma(-t)^\nu, \qquad |t| \to \infty;$$

both $\gamma$ and the exponent $\nu$ are flavor independent. $\alpha_{j\bar{i}}(0) \leq 1$, in accord with the Froissart bound. Note that for $|t| \ll T$, Eq. (5) reduces to the (quasi)linear form

$$\alpha_{j\bar{i}}(t) = \alpha_{j\bar{i}}(0) + \nu\gamma T_{j\bar{i}}^{\nu-1} t = \alpha_{j\bar{i}}(0) + \alpha'_{j\bar{i}}(0)t. \qquad (6)$$

---

[1]Note that the choice of the signs in Eq. (5) is fixed by the requirements that $\alpha(t)$ must be real as $t \to -\infty$, and have positive slope in the small-$t$ region.

The subscripts $i,j$ indicate which of the parameters depend on the quark content of the meson. In this section we drop the subscripts, since our model is applied here to a bottomonium-like system only.

We consider the value of $\nu$ restricted to lie between 0 and 1/2 ( [25], for details see Appendix A). $\nu=0$ should be understood as a limit $\nu \to 0$, $\gamma\nu$ fixed. In this limit, the difference of fractional powers reduces to a logarithm, viz.,

$$\alpha(t) = \alpha(0) - (\gamma\nu)\log\left(1 - \frac{t}{T}\right), \qquad \gamma\nu = \text{const.} \qquad (7)$$

Unlike a trajectory with $\nu \neq 0$, the real part of the "logarithmic" trajectory does not freeze-out when $t$ reaches $T$. The real part continues to grow, the only change for $t > T$ is that the trajectory acquires a constant imaginary part.

The upper bound on $\nu$ gives the so-called "square-root" trajectory, viz.

$$\alpha(t) = \alpha(0) + \gamma[\sqrt{T} - \sqrt{T-t}]. \qquad (8)$$

When $t$ reaches $T$, the real part of the "square-root" trajectory stops growing, and there are no states with a higher angular momentum than $l_{max} = [\alpha(T)]$. The parameter T is therefore the trajectory termination point.

Figure 1(a) shows the parent Regge trajectory for our model together with our best fit of the "square-root" form:

$$\alpha_{\sqrt{}}(0) = -21.12 \pm 7.74,$$

$$\gamma_{\sqrt{}} = 2.68 \pm 0.97 \ [\text{GeV}^{-1}],$$

$$T_{\sqrt{}} = 127.66 \pm 1.98 \ [\text{GeV}^2]$$

$$\chi^2 = 5.86 \times 10^{-2}. \qquad (9)$$

Our best fit of the logarithmic form

$$\alpha_{\log}(0) = -10.89 \pm 7.59,$$

$$(\gamma\nu)_{\log} = 5.0 \pm 3.92,$$

$$T_{\log} = 130.74 \pm 5.39 \ [\text{GeV}^2]$$

$$\chi^2 = 1.45 \times 10^{-2} \qquad (10)$$

is shown in Fig. 1(b). In both cases, the large errors on the extracted parameters reflect the fact that there are only 8 data points for the trajectory.

The two fits are indistinguishable in the region of the fit. In our case, since we *know* that in our model there is only a finite number of bound states, the square-root form (which terminates in general, and in our fit its termination point is near the termination of our bound-state data) is favored over the logarithmic form (which does not terminate). However, in practice, when one has no means to recognize whether the set of data is a part of a finite or an infinite ensemble, it is impossible to distinguish between the two forms based on fits to the bound state data.

In view of this, we extend our considerations on how to numerically determine the form of a Regge trajectory from
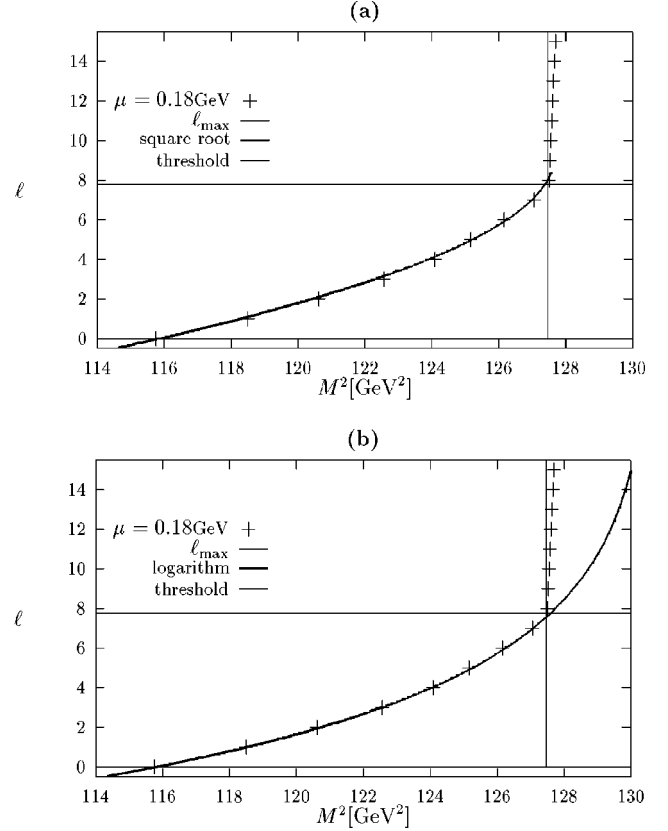


FIG. 1. The parent trajectory for the bottomonium in our model compared to **(a)** our best fit of the "square-root" form, and **(b)** our best fit of the "logarithmic" form. The solid vertical line corresponds to the threshold of the quenched lattice potential, i.e., $(2M + \sigma/\mu)^2$; the solid horizontal line shows the maximum $l$ for the data set.

data. There is more information about Regge trajectories than just the masses of the bound states. Total cross sections can be related to the value of the relevant Regge trajectory at the origin (i.e., the intercept of the trajectory). In the region of negative $t$, the value of $\alpha(t)$ can be determined from the relevant differential cross sections. If there are reliable data at large[2] negative $t$ in addition to bound states, it might be possible to obtain a more stringent constraint on the form of trajectory by fitting both sets of data simultaneously, providing the form is universally valid for all $t$.

## III. ANALYTIC MODEL

Our model calculation for heavy quarks revealed that the Regge trajectory formed by the bound states is certainly non-linear but can be equally well fitted by a square-root form or a logarithmic form.

In this section we try to shed some light on this observation using analytic model for a massless string with variable

---

[2]Unfortunately, according to our numerical simulations, data at larger negative $t$ values, and with greater measurement precision, are both needed.

tension. The ends of the string can be massive. The model is intended to mimic a flux tube stretched between two quarks, and the varrying tension is to reflect possible dynamical effects such as weekening of the flux tube due to pair creation.

The particular merit of the model for our purposes is that, given the form of a Regge trajectory, we are able to recover the form of underlying potential, in many cases in analytic form. We will show in this model why the two forms of Regge trajectories (i.e. square-root and logarithmic) are both likely to well approximate the Regge trajectory formed by the bound states of the unquenched lattice QCD potential (4).

This section is organized as follows: first we review the standard relativistic Nambu-Goto string with massive ends and show that in the nonrelativistic limit this model simply corresponds to a rigid rod with a linear potential generated between its massive ends. After introducing the generalized string model, we show that it corresponds in the nonrelativistic limit to a rigid rod with arbitrary potential. Details for the dynamics of the generalized string with massive ends, such as derivation of expressions for its energy and orbital angular momentum, can be found in the Appendix B. The key part of this section is devoted to the generalized string with massless ends. Within this framework we find potentials that lead to square-root and logarithmic trajectories, respectively. Since the dynamics of mesons (such as the termination of Regge trajectories) is dominated by the behavior of the flux tube, we claim that what we learn from the string with massless ends is qualitatively relevant to the case of massive quarks as well.

### A. The Nambu-Goto string and the generalized string

The action of the standard relativistic Nambu-Goto string with massive ends in the parametrization $\tau=t=x^0$ is written as ($\sigma$ is the string tension) [3]

$$S=-\sigma\int_{t_1}^{t_2}dt\int_0^\pi ds\,\sqrt{x'^2(1-\dot{x}^2)+(\dot{x}x')^2}$$

$$-\sum_{i=1,2}m_i\int_{t_1}^{t_2}dt\,\sqrt{1-\dot{x}_i^2},\qquad(11)$$

$$x\equiv\mathbf{x}=\mathbf{x}(t,s),\quad x_i\equiv x(t,s_i),\quad i=1,2,\quad s_1=0,\quad s_2=\pi,$$

where from now on the dot and the prime stand for the derivative with respect to $t$ and $s$, respectively, unless otherwise specified.

To illuminate the physical meaning of this model, let us consider for the moment its nonrelativistic limit. In the nonrelativistic limit, $|\dot{x}(t,s)|\ll1$, $|\dot{x}_i|\ll1$, and the action reduces to [3]

$$S=-\sigma\int_{t_1}^{t_2}dt\int_0^\pi ds\,\sqrt{x'^2}-\sum_{i=1,2}m_i\int_{t_1}^{t_2}dt+\sum_{i=1,2}\frac{m_i}{2}\int_{t_1}^{t_2}dt\dot{x}_i^2.$$

$$(12)$$

Integration over $s$ gives the length of the string (under the assumption that there are no singularities on the string). The variation of the first term in the nonrelativistic action, Eq.

(11), with respect to the string coordinates leads to the requirement on the string to have the form of a linear rod connecting the massive ends. The effective action that leads to the equations of motion of the massive ends is therefore

$$S_{eff}=\int_{t_1}^{t_2}dt\left(-\sigma|x_1(t)-x_2(t)|+\sum_{i=1,2}\frac{m_i\dot{x}_i^2}{2}\right).\quad(13)$$

Hence, in the nonrelativistic limit, the string generates a linear potential between its massive ends: $V(|x_1-x_2|)=\sigma|x_1-x_2|$.

Here we generalize the standard string formulation described above to the case of an arbitrary potential between the string (strictly as an effective and convenient mathematical representation of a flux tube) massive ends. Such generalization is done by the modification of the standard, constant, string tension into an effective string tension which is a function of $|x|$, as follows:

$$S_{gen}=-\int_{t_1}^{t_2}dt\int_0^\pi ds\,\sigma(|x|)\sqrt{x'^2(1-\dot{x}^2)+(\dot{x}x')^2}$$

$$-\sum_{i=1,2}m_i\int_{t_1}^{t_2}dt\,\sqrt{1-\dot{x}_i^2}.\qquad(14)$$

The action is similar to that of the standard Nambu-Goto string. In the nonrelativistic limit, however, in place of Eq. (13) one will now obtain

$$S_{gen,eff}=\int_{t_1}^{t_2}dt\left(-\int_0^\pi ds\,\sigma(|x|)\sqrt{x'^2}+\sum_{i=1,2}\frac{m_i\dot{x}_i^2}{2}\right)$$

$$=\int_{t_1}^{t_2}dt\left(-V(|x_1-x_2|)+\sum_{i=1,2}\frac{m_i\dot{x}_i^2}{2}\right).\qquad(15)$$

In contrast to the previous case of the standard string, it is seen in the above relations that now

$$\sigma(|x|)=\frac{dV(|x|)}{d|x|},\qquad(16)$$

i.e., the effective string tension is the derivative of a potential with respect to the distance. Obviously, in the case of a linear potential, the effective string tension reduces to the standard (constant) one.

Similarly to the standard case of a constant string tension which represents the relativization inthe manner of Poincaré of the nonrelativistic two-body problem with linear potential [26], the generalized string can be considered as the relativization of a nonrelativistic two-body problem with an arbitrary potential. Details of the dynamics of the generalized string model are given in Appendix B.

### B. Generalized massless string

Since we are interested in dynamical issues related to the properties of the flux tube, without a loss of generality it is sufficient for us to consider the case of a generalized string with massless ends. This case is obviously more tractable

than the case with arbitrary masses, and nevertheless exhibits the same qualitative features.

The energy and orbital momentum of the generalized massless string, $m_1 = m_2 = 0$, is given by

$$E = 2 \int_0^R \frac{d\rho\, \sigma(\rho)}{\sqrt{1 - \omega^2 \rho^2}}, \quad J = 2 \int_0^R \frac{d\rho\, \sigma(\rho)\, \omega \rho^2}{\sqrt{1 - \omega^2 \rho^2}}, \quad (17)$$

where $R = 1/\omega$ is half of the string length for a given $\omega$. The condition $\omega R = 1$ follows from, e.g., Eqs. (B14) with $m_i \to 0$.

By eliminating $\omega$ from Eqs. (17) one can obtain $J$ as a function of $E^2$, the Regge trajectory. It will be shown elsewhere [27] that it is possible to uniquely recover the potential $[V(r) \sim \int d\rho\, \sigma(\rho)]$ from the known analytic form of Regge trajectory, for both massless and massive generalized strings (as representations of flux tubes stretched between both massless and massive quarks, respectively), and the techniques of the corresponding inverse problem will be presented in detail. In this way, we have recovered the potentials that correspond to both the square-root and logarithmic Regge trajectories. For our present purposes, here we present only the final results.

### 1. Square-root trajectory

The potential $[\sigma, \mu = \text{const}, V(\rho) \to \sigma/2\mu$ as $\rho \to \infty$, and hence $E \to \sigma/\mu]$

$$V(\rho) = \frac{\sigma}{\pi\mu} \arctan(\pi\mu\rho), \quad (18)$$

for which

$$\sigma(\rho) = \frac{dV(\rho)}{d\rho} = \frac{\sigma}{1 + (\pi\mu\rho)^2}, \quad (19)$$

leads, via Eq. (17), to

$$E = \frac{\pi\sigma}{\sqrt{\omega^2 + \pi^2 \mu^2}}, \quad J = \frac{\sigma}{\pi\mu^2} \left( 1 - \frac{\omega}{\sqrt{\omega^2 + \pi^2 \mu^2}} \right). \quad (20)$$

Eliminating $\omega$ from the above relations gives

$$J = \frac{1}{\pi\mu} (\sigma/\mu - \sqrt{(\sigma/\mu)^2 - E^2}), \quad (21)$$

i.e., the square-root Regge trajectory. For $E \ll \sigma/\mu$, it reduces to an (approximate) linear trajectory, $J \simeq E^2/(2\pi\sigma)$.

### 2. Logarithmic trajectory

The potential

$$V(\rho) = \frac{\sigma}{2\pi\mu} \left( 2 \arctan(2\pi\mu\rho) - \frac{\log[1 + (2\pi\mu\rho)^2]}{2\pi\mu\rho} \right), \quad (22)$$
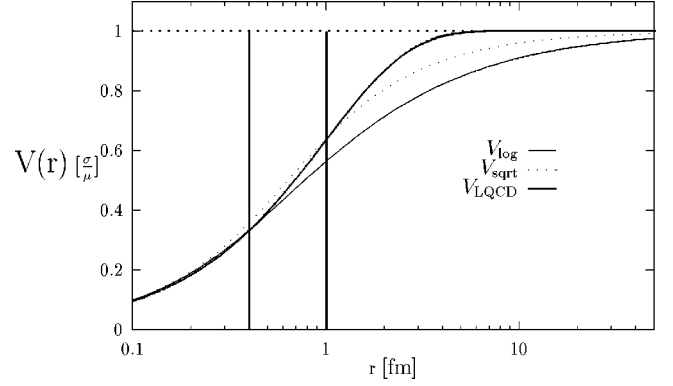
for which



FIG. 2. Potentials which in our analytical model lead to logarithmic and square-root Regge trajectories, respectively, compared to the unquenched lattice QCD potential used in our heavy-quarkonia calculation.

$$\sigma(\rho) = \sigma \frac{\log[1 + (2\pi\mu\rho)^2]}{(2\pi\mu\rho)^2}, \quad (23)$$

leads to

$$E = \frac{\sigma}{2\pi\mu^2} (\sqrt{\omega^2 + 4\pi^2\mu^2} - \omega),$$

$$J = \frac{\sigma}{2\pi\mu^2} \log \frac{\omega + \sqrt{\omega^2 + 4\pi^2\mu^2}}{2\omega}, \quad (24)$$

from which eliminating $\omega$ [viz., $\omega = \pi(\sigma^2 - \mu^2 E^2)/(\sigma E)$] gives

$$J = -\frac{\sigma}{2\pi\mu^2} \log \left( 1 - \frac{E^2}{(\sigma/\mu)^2} \right), \quad (25)$$

i.e., the logarithmic Regge trajectory. For $E \ll \sigma/\mu$, it again reduces to an (approximate) linear form, $J \simeq E^2/(2\pi\sigma)$.

Figure 2 shows both potentials together with the confining part of the screened lattice QCD potential that we used in the heavy quark model in the previous section. All potentials are normalized to the same asymptotic value. The vertical lines show the region of the distance $r$ which is relevant for the bound states.

All three potentials are very close in the region of bound state physics. Therefore, one can conclude that they would lead to similar Regge trajectories as far as the bound states not close to the trajectory thresholds are concerned. One could further speculate that since the lattice potential is steeper than the square-root potential (which in turn, is steeper than the logarithmic potential) in asymptotia, it is reasonable to expect that the bound states of the lattice potential terminate at a lower $l$ than the square-root trajectory, and that the square-root trajectory approximates the lattice potential trajectory better for states near the trajectory threshold than the logarithmic trajectory. (Recall that the real part of the logarithmic trajectory does not terminate.)

Combining the conclusions of the analytic model for the generalized string with those of the heavy quark model of the previous section, we conclude that even though both nonlinear forms considered may appear to be a good approximation to QCD, the square-root form is likely to be more realistic. Therefore, we use the square-root form for phenomenological purposes.

## IV. TRAJECTORY PARAMETERS AND SPECTROSCOPY

In this section we determine, assuming that Regge trajectories are of the form (8), trajectories thresholds and intercepts using various experimental information. Typically, we use masses of a few known lowest lying states, and in the case of the $\rho$ trajectory we also use the value of the intercept (which is known and well-established) found from exchange processes. The value of $\gamma$ (the universal asymptotic slope) is fit to the $\rho$ trajectory, and then taken as universal for all other trajectories.

Whenever possible, we try to use as inputs states that are believed to be pure quark-antiquark states with definite flavors. For example, we do not use the masses of the observed $\phi$, $f$ or $\eta(\eta')$ states to find the parameters of $s\bar{s}$ trajectory because the physical states are mixtures of $s\bar{s}$ with the light quark-antiquark components.

In some cases, e.g. for tensor mesons and axial-vector mesons, there are not enough data to determine the parameters. We are forced to make aditional assumptions. In particular, we assume that the thresholds of parity partner trajectories coincide. We comment further on this assumption where it is introduced in Sec. IV B. Here we wish to mention that our additional assumptions are justified *a posteriori* by our excellent results.

The approach has more predictive power than one would naively expect. This is because the parameters for different flavors are related by
(i) additivity of intercepts,

$$\alpha_{i\bar{i}}(0)+\alpha_{j\bar{j}}(0)=2\alpha_{j\bar{i}}(0), \tag{26}$$

where $i,j(\bar{i},\bar{j})$ refer to the quark (antiquark) flavor,[3] and
(ii) additivity of inverse slopes near the origin,

$$\frac{1}{\alpha'_{i\bar{i}}}+\frac{1}{\alpha'_{j\bar{j}}}=\frac{2}{\alpha'_{j\bar{i}}}, \tag{27}$$

which is favored over another constraint suggested in the literature, factorization of slopes, $\alpha'_{i\bar{i}}\alpha'_{j\bar{j}}=(\alpha'_{j\bar{i}})^2$, by the heavy quark limit [28]. These two additivity requirements are independent of which specific form is assumed for the trajectories.

Once the parameters of the square-root trajectories are known, the first obvious application is meson spectroscopy. We calculate masses of a few excited states lying on each of

---

[3]This additivity is a firmly established theoretical constraint on Regge trajectories (for an extensive list of references see [28]).

the trajectories under consideration, and compare with experimental data from Ref. [29]. Where there are no data available, our results are predictions.

We start with vector meson trajectories, and then consider tensor meson, pseudoscalar meson, and finally, axial-vector meson trajectories. The section concludes with a brief discussion of the results.

### A. Vector mesons

We start with the $\rho$ trajectory. The intercept of this trajectory is well established. From the behavior of the differential cross section of the process $\pi^-p\rightarrow\pi^0n$ the intercept $\alpha_\rho(0)$ has been extracted to be 0.58 [30], $0.56\pm0.01$ [31], $0.56\pm0.02$ [32], 0.53 [33]. Extensive analysis of this process by Höhler *et al.* [34] leads to $\alpha_\rho(0)=0.55$ [35]. From the difference of the total cross sections of $\pi^+p$ and $\pi^-p$ scattering $\alpha_\rho(0)$ has been inferred to be $0.57\pm0.01$ [36], $0.55\pm0.03$ [37]. Bouquet finds from the dual topological unitarization [38] $0.51\leqslant\alpha_\rho(0)\leqslant0.54$. All of the above values are consistent with

$$\alpha_\rho(0)=0.55, \tag{28}$$

in agreement with the value of the $\rho$ trajectory intercept extracted by Donnachie and Landshoff from the analysis of $pp$ and $\bar{p}p$ scattering data in a simple pole exchange model [39]. We therefore take the value of the intercept, Eq. (28) as one of the constraints on the form of the $\rho$ trajectory. Two more constraints that are needed are provided by the mass and spin of $\rho$ and $\rho_3$, i.e., (i) $\alpha_\rho(M_\rho^2)=1$, (ii) $\alpha_\rho(M_{\rho_3}^2)=3$, where $M_\rho=769.0\pm0.9$ MeV and $M_{\rho_3}=1688.8\pm2.1$ MeV [29].

Inserting these values into the functional form (8), we extract the parameter values

$$\gamma=3.65\pm0.05 \text{ GeV}^{-1}, \quad \sqrt{T_\rho}=2.46\pm0.03 \text{ GeV}. \tag{29}$$

It is interesting to note that the values of parameters we find based on spectroscopy and the known intercept are in excellent agreement with

$$\gamma=3.72\pm0.30 \text{ GeV}^{-1}, \quad \sqrt{T_\rho}=2.50\pm0.10 \text{ GeV}, \tag{30}$$

extracted in Ref. [40] for a similar form of the $\rho$ trajectory from the analysis of $\pi N$ charge-exchange scattering data.[4] Earlier analysis of Ref. [41] found $\sqrt{T_\rho}=2.4\pm0.4$ GeV.

The parameters of the $K^*$ trajectory are obtained by using $\alpha_{K*}(M_{K*}^2)=1$ with $M_{K*0}=896.1\pm0.3$ MeV and $\alpha_{K*}(M_{K_3^*}^2)=3$ with $M_{K_3^{*0}}=1776\pm7$ MeV [29], and taking the value of $\gamma$ found from $\rho$ spectra as a universal slope in asymptopia. This yields

---

[4]The $\rho$ trajectory adopted in [40] contains an additional term $-0.14\sqrt{4M_\pi^2-t}$, to take into account nonzero resonance widths, which reduces the planar intercept $\alpha_\rho(0)$ down to 0.51.

TABLE I. Parameters of the vector meson trajectories of the form (8). The intercept of the $\rho$ trajectory was taken as an input.

|  | $\rho$ | $K^*$ | $\phi$ |  |
|---|---|---|---|---|
| $\alpha(0)$ | 0.55 | $0.414 \pm 0.006$ | $0.27 \pm 0.01$ |  |
| $\sqrt{T}$, GeV | $2.46 \pm 0.03$ | $2.58 \pm 0.03$ | $2.70 \pm 0.07$ |  |
|  | $D^*$ | $D_s^*$ | $J/\psi$ |  |
| $\alpha(0)$ | $-1.02 \pm 0.05$ | $-1.16 \pm 0.05$ | $-2.60 \pm 0.10$ |  |
| $\sqrt{T}$, GeV | $3.91 \pm 0.02$ | $4.03 \pm 0.04$ | $5.36 \pm 0.05$ |  |
|  | $B^*$ | $B_s^*$ | $B_c^*$ | $\Upsilon$ |
| $\alpha(0)$ | $-7.13 \pm 0.17$ | $-7.27 \pm 0.17$ | $-8.70 \pm 0.18$ | $-14.81 \pm 0.35$ |
| $\sqrt{T}$, GeV | $7.48 \pm 0.02$ | $7.60 \pm 0.04$ | $8.93 \pm 0.03$ | $12.50 \pm 0.02$ |

$$\sqrt{T_{K*}} = 2.58 \pm 0.03 \ \text{GeV}.$$

$$\alpha_{K*}(0) = 0.414 \pm 0.006. \tag{31}$$

The value of the intercept is in an excellent agreement with the results of the analysis of hypercharge exchange processes $\pi^+ p \to K^+ \Sigma^+$ and $K^- p \to \pi^- \Sigma^+$ [42].

Taking the parameters of the $\rho$ and $K^*$ trajectories as known, those for the $\phi$ trajectory may be obtained from the requirements of additivity of inverse slopes and intercepts, Eqs. (26),(27):

$$\alpha_\phi(0) = 0.25 \pm 0.02,$$

$$\sqrt{T_\phi} = 2.59 \pm 0.11 \ \text{GeV}. \tag{32}$$

Similarly, one can obtain the parameters of trajectories for the states containing $c$- and $b$-quarks, using the value of the universal slope $\gamma$ found from $\rho$-trajectory and masses of the corresponding states. In particular, we use masses of $D^*$, $J/\psi$, $B^*$ and $\Upsilon$ as inputs. The remaining trajectories are determined from the requirements of additivity of inverse slopes and of additivity of intercepts, Eqs. (26), (27). The parameters of these vector meson trajectories are summarized in Table I.

Using the parameters shown in Table I, we calculate masses of the spin-1, spin-3 and spin-5 states lying on these trajectories. Our results are compared with data from [29] in Table II. In this, and subsequent Tables IV, VI, VIII, the values used as input for our analysis are shown in boldface. The masses of the states for which there are no data available should be considered as our predictions.

### B. Tensor meson trajectories

Tensor meson trajectories are parity partners of the vector meson trajectories. In a nonrelativistic theory, tensor meson trajectories are degenerate with vector meson trajectories. In a field theory, both acquire different corrections to the intercept, but they can still be expected nearly degenerate in the bound state region. From the form of the trajectory, Eq. (8), and since the intercept is in practice much smaller than the other terms in Eq. (8), it is clear that trajectories can be near-degenerate in the bound-state region even if their intercepts differ by a large percentage, but not if their thresholds are very different. For this reason, and to reduce the number of free parameters, we *assume* that the thresholds of tensor meson trajectories are the same as the thresholds of the vector meson ones.

Our assumption is supported by analysis of the processes $\pi^+ p \to K^+ \Sigma^+$ and $K^- p \to \pi^- \Sigma^+$ [42]. Most of the analyzed experiments show the same slope at the origin for $K^*$ and $K_2^*$ trajectories. In our formalism, this translates to equal thresholds.

TABLE II. Comparison of the masses of the spin-1, spin-3 and spin-5 states given by ten vector meson trajectories of the form (8) with data. All masses are in MeV.

|  | $J=1$ | | $J=3$ | | $J=5$ | |
|---|---|---|---|---|---|---|
|  | This work | Ref. [29] | This work | Ref. [29] | This work | Ref. [29] |
| $\alpha_\rho(t)$ | **769.0±0.9** | 769.0±0.9 | **1688.8±2.1** | 1688.8±2.1 | 2124±19 | |
| $\alpha_{K*}(t)$ | **896.1±0.3** | 896.1±0.3 | **1776±7** | 1776±7 | 2215±21 | |
| $\alpha_\phi(t)$ | 1015±17 | 1019.4 | 1863±31 | 1854±7 | 2305±42 | |
| $\alpha_{D*}(t)$ | **2006.7±0.5** | 2006.7±0.5 | 2721±23 | | 3191±22 | |
| $\alpha_{D_s^*}(t)$ | 2102±29 | 2106.6±2.1±2.7 | 2808±28 | | 3279±30 | |
| $\alpha_{J/\psi}(t)$ | **3096.9** | 3096.9 | 3753±41 | | 4240±39 | |
| $\alpha_{B*}(t)$ | **5324.9±1.8** | 5324.9±1.8 | 5814±51 | | 6217±46 | |
| $\alpha_{B_s^*}(t)$ | 5411±58 | 5416.3±3.3 | 5901±53 | | 6306±49 | |
| $\alpha_{B_c^*}(t)$ | 6356±80 | | 6853±72 | | 7276±65 | |
| $\alpha_\Upsilon(t)$ | **9460.4±0.2** | 9460.4±0.2 | 9906±91 | | 10304±84 | |

TABLE III. Parameters of tensor meson trajectories of the form (8).

|  | $a_2$ | $K_2^*$ | $f_2'$ |  |
| --- | --- | --- | --- | --- |
| $\alpha(0)$ | $0.60\pm0.03$ | $0.42\pm0.03$ | $0.22\pm0.07$ |  |
|  | $D_2^*$ | $D_{s2}^*$ | $\chi_{c2}(1P)$ |  |
| $\alpha(0)$ | $-1.16\pm0.05$ | $-1.35\pm0.05$ | $-2.93\pm0.09$ |  |
|  | $B_2^*$ | $B_{s2}^*$ | $B_{c2}^*$ | $\chi_{b2}(1P)$ |
| $\alpha(0)$ | $-7.62\pm0.13$ | $-7.81\pm0.13$ | $-9.39\pm0.14$ | $-15.85\pm0.26$ |

To further test this assumption, we first fit the threshold of the $K_2^*$ trajectory which is the only one with more than one state. (A recent measurement of the $a_4$ mass [43,44] is four standard deviations below the previous value [29], see discussion in the text below.) The parameters of the $K_2^*$ trajectory are fixed by using $\gamma$ determined for $\rho$ trajectory, $\alpha_{K_2^*}(M_{K_2^*}^2)=2$ with $M_{K_2^{*0}}=1432.4\pm1.0$ MeV and $\alpha_{K_2^*}(M_{K_4^*}^2)=2$ with $M_{K_4^{*0}}=2045\pm9$ MeV [29]. The calculation yields

$$\sqrt{T_{K_2^*}}=2.64\pm0.03 \text{ GeV}. \tag{33}$$

The value of the $K_2^*$ trajectory threshold is consistent with that of the $K^*$ trajectory given in Table I, supporting our assumption. Moreover, it is in excellent agreement with the values for the slope shown in Ref. [42].

We therefore conclude that our assumption that the thresholds of the parity partners are the same is plausible. Under this simplifying assumption only one state on each trajectory is needed to completely fix the parameters. We choose to fit $a_2$, $K_2^*$, $\chi_{c2}$ and $\chi_{b2}$ trajectories using the masses of the corresponding lowest lying state. The remaining trajectories are determined using the addititivity requirements. Parameters found in this way are presented in Table III.

As before, we use the knowledge of Regge trajectories for spectroscopy purposes. Our results are compared with data from [29] in Table IV. The masses of the states for which there are no data available should again be considered our predictions.

Note that all the masses agree very well for the available data, except for $M_{a_4}$. With respect to this, we wish to mention that recent analyses by the VES Collaboration of the reactions $\pi^-\text{Be}\to\pi^+2\pi^-2\pi^0\text{Be}$ [43] and $\pi^-\text{Be}\to\pi^+2\pi^-2\text{Be}$ [44] reveal the mass of the $a_4$ resonance as seen in the $a_4\to\omega\rho$ and $a_4\to f_2\pi$ decays, respectively: $1944\pm8\pm50$ MeV [43] and $1950\pm20$ MeV [44]. Our value in Table IV is in excellent agreement with these latest measurements.

According to our fitted square-root form for the $a_2$ trajectory, the last state below threshold is $J=8$. This conclusion is very sensitive to the functional form assumed, even though the threshold value itself is not (see Sec. II). Generally, as the mass approaches the threshold, we expect to find larger discrepancies between the observed states and predictions of any specific form of trajectory, Eq. (5). Nonetheless, the discrepancy for the next-to-last, $J=6$ state appears to be less than 10%. Note also that our $K_4^*$ prediction appears to be below the data, consistent with $a_4$ and $a_6$ deviations, suggesting a possible systematic effect. This raises the possibility that the growth of the square-root form of trajectory near the termination point is too rapid and that the true trajectories are somewhat flatter in this region. Thus, it is possible that the $J=6$ state is actually the last state on these trajectories. This point of view is further supported by the large width of the $a_6$, as would be expected for a state near the termination point. Hence we also expect the $K_6^*$ to be similarly broad.

### C. Pseudoscalar meson trajectories

Here we calculate the parameters of the pseudoscalar meson trajectories. We start with the pion trajectory and fix its intercept and threshold by using the masses of the two lowest lying states, $M_{\pi^0}=135$ MeV and $M_{\pi_2}=1677\pm8$ MeV [29], in relations $\alpha_\pi(M_\pi^2)=0$, $\alpha_{-\pi}(M_{\pi_2}^2)=2$, and $\gamma$ from Eq. (29).

Similarly, the intercept and the threshold of the $K$-trajectory are determined using the massses of $K$ and $K_2$.

TABLE IV. Comparison of the masses of the spin-2, spin-4 and spin-6 states given by ten tensor meson trajectories of the form (8) with data. All masses are in MeV. See the text regarding the $a_4$ and $a_6$ masses.

|  | $J=2$ | | $J=4$ | | $J=6$ | |
| --- | --- | --- | --- | --- | --- | --- |
|  | This work | Ref. [29] | This work | Ref. [29] | This work | Ref. [29] |
| $\alpha_{a_2}(t)$ | **1318.1±0.6** | 1318.1±0.6 | 1927±18 | 2020±16 | 2256±21 | 2450±130 |
| $\alpha_{K_2^*}(t)$ | **1432.4±1.3** | 1432.4±1.3 | 2026±20 | 2045±9 | 2357±24 | |
| $\alpha_{f_2'}(t)$ | 1544±37 | 1525±5 | 2124±40 | | 2457±48 | |
| $\alpha_{D_2^*}(t)$ | 2454±23 | 2458.9±2.0 | 3010±22 | | 3390±21 | |
| $\alpha_{D_{s2}^*}(t)$ | 2560±27 | 2573.5±1.7 | 3109±29 | | 3489±31 | |
| $\alpha_{\chi_{c2}(1P)}(t)$ | **3556.2±0.1** | 3556.2±0.1 | 4092±39 | | 4498±38 | |
| $\alpha_{B_2^*}(t)$ | 5698±45 | 5698±12 | 6122±42 | | 6472±39 | |
| $\alpha_{B_{s2}^*}(t)$ | 5797±47 | | 6220±45 | | 6570±43 | |
| $\alpha_{B_{c2}^*}(t)$ | 6780±52 | | 7213±50 | | 7582±49 | |
| $\alpha_{\chi_{b2}(1P)}(t)$ | **9913.2±0.6** | 9913.2±0.6 | 10310±72 | | 10665±68 | |

TABLE V. Parameters of the pseudoscalar meson trajectories of the form (8). (The parameters for the $K$ trajectory were found using the mass of $K_2$ from [29]. If we instead use a mass of the corresponding *pure $n\bar{s}$* state as found in Ref. [46], i.e., $M_{K_2} = 1762 \pm 18$ GeV, the parameters change slightly: the intercept $-0.153 \pm 0.003$, and the threshold $2.93 \pm 0.07$ GeV.)

| | $\pi$ | $K$ | $\eta_s$ | |
|---|---|---|---|---|
| $\alpha(0)$ | $-0.0118 \pm 0.0001$ | $-0.151 \pm 0.001$ | $-0.291 \pm 0.003$ | |
| $\sqrt{T}$, GeV | $2.82 \pm 0.05$ | $2.96 \pm 0.05$ | $3.10 \pm 0.11$ | |
| | $D$ | $D_s$ | $\eta_c$ | |
| $\alpha(0)$ | $-1.61105 \pm 0.00005$ | $-1.751 \pm 0.001$ | $-3.2103 \pm 0.0001$ | |
| $\sqrt{T}$, GeV | $4.16 \pm 0.03$ | $4.29 \pm 0.06$ | $5.49 \pm 0.02$ | |
| | $B$ | $B_s$ | $B_c$ | $\eta_c$ |
| $\alpha(0)$ | $-7.41 \pm 0.17$ | $-7.54 \pm 0.17$ | $9.00 \pm 0.17$ | $-14.80 \pm 0.34$ |
| $\sqrt{T}$, GeV | $7.89 \pm 0.16$ | $8.01 \pm 0.16$ | $9.24 \pm 0.12$ | $12.98 \pm 0.24$ |

The parameters of charmed mesons trajectories are found using the masses of $D$ and $\eta_c$, utilizing the additivity requirements, Eqs. (26),(27), and the parameters of the light mesons ($\pi$-trajectory) found above.

If one tries to procceed similarly in the case of mesons containing the $b$ quark, and use the only two experimentally known masses as inputs (the mass of $B$ and $B_s$) in conjunction with the parameters of $\pi$- and $K$-trajectory, the error estimates on the extracted values exceed two hundred percent. The results turn out to be highly unstable with respect to the threshold of the $\pi$-trajectory. This is a peculiar consequence of the pion intercept being close to zero, and $J=0$ of the lowest lying state.

Conversely, this observation allows us to convert the problem into an additional self-consistency check. We use the $b$-quark meson spectra to extract information about the $\pi$ trajectory. To do that, an additional input is needed. We use the mass of $\eta_b$ given in Ref. [45], and fit the value of the pion threshold in addition to the parameters of $b$-containing mesons. Recall that the light meson parameters affect the heavy quark parameters only through the additivity requirements. Since the additivity requirements are well established, such a self-consistency check is quite nontrivial.

The parameters of the pseudoscalar trajectories that we obtain are shown in Table V. The parameters of the $\pi$-trajectory given in the table come from fitting the pion spectra. From the bottom spectra we obtain the following value of the pion threshold:

$$\sqrt{T_\pi} = 2.79 \pm 0.40 \text{ GeV.} \tag{34}$$

Note the agreement with the value given in Table V.

Our results for pseudoscalar spectroscopy are compared with data from [29] in Table VI. The masses of the states for which there are no data available should once again be considered our predictions.

### D. Axial-vector meson trajectories

Finally, we calculate the parameters of the axial-vector trajectories. These have the same parity and spin as the parity partners of the pseudoscalar trajectories—the pseudovector

TABLE VI. Comparison of the masses of the spin-0, spin-2 and spin-4 states given by ten pseudoscalar meson trajectories of the form (8) with data. (We take the error estimate on the $\eta_b$ mass as 10% of the calculated splitting, in agreement with Fig. 2 of the second paper of Ref. [45].) All masses are in MeV.

| | $J=0$ | | $J=2$ | | $J=4$ | |
|---|---|---|---|---|---|---|
| | This work | Ref. [29] | This work | Ref. [29] | This work | Ref. [29] |
| $\alpha_\pi(t)$ | **135** | 135 | **$1677 \pm 8$** | $1677 \pm 8$ | $2237 \pm 26$ | |
| $\alpha_K(t)$ | **493.7** | 493.7 | **$1773 \pm 8$** | $1773 \pm 8$ | $2333 \pm 27$ | |
| $\alpha_{\eta_s}$ | $698 \pm 14$ | | $1869 \pm 38$ | $1854 \pm 20$ | $2429 \pm 54$ | |
| $\alpha_D(t)$ | **$1864.1 \pm 1.0$** | $1864.1 \pm 1.0$ | $2692 \pm 19$ | | $3228 \pm 22$ | |
| $\alpha_{D_s}(t)$ | $1971 \pm 19$ | $1969.0 \pm 1.4$ | $2786 \pm 26$ | | $3323 \pm 32$ | |
| $\alpha_{\eta_c}(t)$ | **$2979.8 \pm 2.1$** | $2979.8 \pm 2.1$ | $3692 \pm 23$ | | $4217 \pm 25$ | |
| $\alpha_B(t)$ | **$5279.8 \pm 1.6$** | $5279.8 \pm 1.6$ | $5830 \pm 89$ | | $6286 \pm 93$ | |
| $\alpha_{B_s}(t)$ | **$5369.6 \pm 2.4$** | $5369.6 \pm 2.4$ | $5920 \pm 89$ | | $6376 \pm 93$ | |
| $\alpha_{B_c}(t)$ | $6283 \pm 79$ | | $6826 \pm 79$ | | $7287 \pm 80$ | |
| $\alpha_{\eta_b}(t)$ | **$9424 \pm 3.6$** | | $9914 \pm 148$ | | $10353 \pm 150$ | |

TABLE VII. Parameters of axial-vector meson trajectories of the form (8).

|  | $a_1$ | $K_1$ | $f_1'$ |  |
|---|---|---|---|---|
| $\alpha(0)$ | $-0.03\pm0.07$ | $-0.22\pm0.08$ | $-0.42\pm0.15$ |  |
|  | $D_1$ | $D_{s1}$ | $\chi_{c1}(1P)$ |  |
| $\alpha(0)$ | $-1.83\pm0.05$ | $-2.03\pm0.06$ | $-3.63\pm0.07$ |  |
|  | $B_1^*$ | $B_{s1}$ | $B_{c1}$ | $\chi_{b1}(1P)$ |
| $\alpha(0)$ | $-7.87\pm0.27$ | $-8.06\pm0.28$ | $-9.67\pm0.27$ | $-15.70\pm0.54$ |

trajectories.[5] The available data are insufficient to fix both thresholds and intercepts of axial-vector trajectories. We assume, therefore, in analogy with the tensor vs vector meson trajectories, that the thresholds of the parity partners coincide, and further, that the thresholds do not depend on charge conjugation in accordance with the $C$-invariance of QCD. Under this assumption, we use the calculated thresholds of pseudoscalar trajectories and fit only the intercepts of the axial-vector trajectories using the masses of a few lowest lying states and/or the additivity requirements, Eqs. (26),(27).

In particular, we use masses of $a_1$, $D_{s1}$, $\chi_{c1}(1P)$ and $\chi_{b1}(1P)$. Note, that to find the parameters of trajectories of mesons containing strangeness, we use in the absence of data for $K_1$ the mass of $D_s$ rather than $f_1'$. This is because the $f_1'$ is not a pure $s\bar{s}$ state, and therefore the value of the intercept extracted from the physical state could deviate significantly from the value corresponding to a pure $s\bar{s}$ trajectory. (An additional complication arises, in principle, for axial mesons since the physical $q\bar{q}'$ states are mixtures of axial-vector and pseudovector components, because charge conjugation is not well-defined for other than $q\bar{q}$ states. Note that for all states other than axial-vector mesons, the corresponding state with opposite $C$ is exotic, so that the problem is avoided. Of the inputs we use, this is relevant only to $D_{s1}$. We assume that the masses of $D_{s1A}$ and $D_{s1B}$ are close, because the heavy

quark content implies that the hyperfine mass splitting is small.)

As before, $\gamma$ is taken as universal, and the value found from the $\rho$ trajectory is used. The parameters we obtain in this way are in Table VII.

Our results for masses of the states lying on the resulting trajectories are compared with data from [29] in Table VIII. The masses of the states for which there are no data available should, as before, be considered as our predictions.

### E. Discussion of the results

Here we comment on the results presented in this section.

#### 1. Intercepts

*Light-quark ($n\bar{n}$) trajectories:*
(i) The intercept of the linear trajectory that passes through $\rho$ and $\rho_3$, $\alpha(t)=0.48+0.88t$, should be reduced for the $a_2$ if the $a_2$ were on a parallel linear trajectory: $0.47+0.88t$. Even lower value for the intercept (and a different value of the slope), $0.30+0.98t$, is needed if $a_2$ and $a_4$ masses were to lie on the same linear trajectory (the latter being 1.944 MeV, in accord with VES's recent measurements [43]). (Note the discrepancy between the two sets of the $a_2$ trajectory parameters.) In our case, due to nonlinearity the intercept increases to 0.55 for $\rho$ and $0.60\pm0.03$ for $a_2$. The data on $pp$, $\bar{p}p$ [47] undoubtedly show that the tensor intercept is larger than the vector one (although the numerical errors of these data prevent us from using them as input). Therefore, data disfavor a linear trajectory.

(ii) The value $\alpha_{a_2}(0)=0.60\pm0.03$ that we obtain here is in agreement with the recent reanalysis by Cudell, Kang and Kim [47] of the $pp$ and $\bar{p}p$ scattering data in the simple pole exchange model [39] $\alpha_\rho(0)=0.50\pm0.07$, $\alpha_{a_2}(0)=0.66\pm0.08$. In this analysis the pairs of trajectories, $\rho$ and $\omega$, and $a_2$ and $f_2$, are taken to be degenerate. However, since $M(\omega)>M(\rho)$ and $M(f_2)>M(a_2)$, the intercepts of these

TABLE VIII. Comparison of the masses of the spin-1, spin-3 and spin-5 states given by ten axial-vector meson trajectories of the form (8) with data. All masses are in MeV.

|  | $J=1$ | | $J=3$ | | $J=5$ | |
|---|---|---|---|---|---|---|
|  | This work | Ref. [29] | This work | Ref. [29] | This work | Ref. [29] |
| $\alpha_{a_1}(t)$ | **1230±40** | 1230±40 | 2000±31 |  | 2427±32 |  |
| $\alpha_{K_{1A}}(t)$ | 1368±46 |  | 2109±33 |  | 2535±33 |  |
| $\alpha_{f_1}(t)$ | 1501±78 | 1518±5 | 2218±62 |  | 2643±67 |  |
| $\alpha_{D_1}(t)$ | 2418±26 | 2422.2±1.8 | 3042±25 |  | 3473±24 |  |
| $\alpha_{D_{s1}}(t)$ | **2535.4±0.3** | 2535.4±0.3 | 3150±34 |  | 3580±37 |  |
| $\alpha_{\chi_{c1}(1P)}(t)$ | **3510.5±0.1** | 3510.5±0.1 | 4080±30 |  | 4513±28 |  |
| $\alpha_{B_1}(t)$ | 5692±104 |  | 6171±102 |  | 6570±104 |  |
| $\alpha_{B_{s1}}(t)$ | 5796±105 |  | 6273±104 |  | 6671±105 |  |
| $\alpha_{B_{c1}}(t)$ | 6740±95 |  | 7215±92 |  | 7620±90 |  |
| $\alpha_{\chi_{b1}(1P)}(t)$ | **9891.9±0.7** | 9891.9±0.7 | 10333±173 |  | 10727±172 |  |

---

[5]We use the usual Regge terminology for parity partners, which is not the same as normally used in lattice QCD/chiral condensates.

trajectories should actually satisfy $\alpha_\omega(0) < \alpha_\rho(0)$ and $\alpha_{a_2}(0) < \alpha_{f_2}(0)$. Hence, the value of $\alpha_\rho(0)$ should be larger than the average of $\alpha_\rho(0)$ and $\alpha_\omega(0)$, i.e., 0.50. Similarly, the value of $\alpha_{a_2}(0)$ should be less than 0.66.

Our values for the intercepts agree well with their values within the errors, moreover, they satisfy the above described inequalities.

(iii) Our value $\alpha_{a_1}(0) = -0.03 \pm 0.07$ is consistent with $\alpha_{a_1}(0) = -0.1 \pm 0.2$ found in the analysis of the reaction $\pi^- p \to \pi^- \pi^+ n$ [48].

*Trajectories containing strangeness:*
The values of $K^*$ and $K_2^*$ intercepts are in excellent agreement with the analysis of hypercharge exchange processes $\pi^+ p \to K^+ \Sigma^+$ and $K^- p \to \pi^- \Sigma^+$ [42].

*Trajectories containing a heavy quark:*
(i) The calculated intercepts of the heavy quark trajectories are negative, and the absolute value of an intercept increases with the increasing mass of the heavy quark. This feature is confirmed by means of the operator expansion of QCD and dispersion relations for heavy quark four-current correlation functions by Oganesyan and Khodzhamiryan [49]. They also find the estimates $\alpha_{J/\psi}(0) \sim -(2-3)$, $\alpha_\Upsilon(0) < -10$. Our corresponding results, $\alpha_{J/\psi}(0) = -2.60 \pm 0.1$ and $\alpha_\Upsilon(0) = -14.81 \pm 0.35$, agree very well with these estimates provided by QCD.

(ii) Our predictions for the intercepts of the charmed meson trajectories may be confronted with the existing data. For the reaction

$$\pi^- A \to D(D^*) X$$

the differential cross section, as given in the triple-Regge limit [50], is

$$\frac{d^2\sigma}{dx_F dp_\perp^2} = A(1 - |x_F|)^n e^{-bp_\perp^2}, \quad A, b = \text{const},$$

where $x_F$ and $p_\perp$ are the Feynman-$x$ and transverse momentum variables, respectively, and $n = 1 - 2\alpha(0)$, with $\alpha(0)$ being the intercept of the trajectory exchanged in the $t$-channel of the reaction. The $D$ meson production proceeds via the exchange of both $D^*$ and $D_2^*$ trajectories. Hence, on the basis of our results for the corresponding intercepts, one may expect $n \simeq 3.2 \pm 0.2$ for the $D$-production. In $\pi^- H$ interactions at 360 GeV the NA27 experiment by the LEBC-EHS Collaboration [51] finds $n = 3.80 \pm 0.63$. For 350 GeV $\pi^-$ beam on emulsion the WA75 Collaboration [52] finds $n = 3.5 \pm 0.5$. In $\pi^- Cu$ interactions at 230 GeV the ACCMOR Collaboration [53] finds $n = 3.23 \pm 0.29$ for leading charm production (and $n = 4.34 \pm 0.35$ for nonleading, and $n = 3.74 \pm 0.23$ for the combined data). For 340 GeV $\pi^-$ beam on Si, Cu and W targets the WA82 Collaboration [54] finds $n = 2.9 \pm 0.3$. Finally, for 250 GeV $\pi^-$ beam on Be, Al, Cu and W targets the E769 Collaboration [55] finds $n = 3.2 \pm 0.5$ on Al target, and $n = 3.7 \pm 0.4$ for leading $D$ production on all targets (and $n = 4.0 \pm 0.4$ for nonleading, and $n = 3.9 \pm 0.3$ for the combined data).

Since the $D^*$ meson production can proceed via the exchanges of all four, $D^*$, $D_2^*$, $D$ and $D_1$, trajectories calculated here, definite predictions for $n$ are more complicated than in the previous case. Of course, quantitatively $n$ should be larger in this case, because the intercepts of $D$ and $D_1$ trajectories are larger in magnitude than those of $D^*$ and $D_2^*$ trajectories. In fact, in the experiment mentioned above the E769 collaboration [56] finds $n = 3.5 \pm 0.3$. Earlier measurements in the NA27 experiment [51] produced $n = 4.3^{+1.8}_{-1.5}$.

The value $\alpha_{D*}(0) = -1.02 \pm 0.05 \approx -1$ obtained in our analysis also supports the use of the $(1 - |x_F|)^3$ production model which was claimed to describe the available data reasonably well [57].

### 2. Spectroscopy

(i) *Masses of $s\bar{s}$ states.* Our predictions for the masses of pure $s\bar{s}$ states cannot be directly compared to the values for physical states quoted by [29], because the physical states emerge upon mixing with the nonstrange isoscalar states of the corresponding meson multiplets. Comparison should be therefore made with the pure $s\bar{s}$ states calculated from both the established physical $n\bar{n}$ and $s\bar{s}$ states. Pure $s\bar{s}$ states were calculated in [58] with the help of Schwinger's quartic mass formula, for both linear and quadratic masses, in essential agreement in both cases and consistent with the quark model motivated linear mass relation $M(n\bar{n}) + M(s\bar{s}) = 2M(s\bar{n})$. Here we quote the masses of the pure $s\bar{s}$ states found in [58] (specifically, from Schwinger's formula for quadratic masses) for vector $J = 1,3$, tensor $J = 2$ and pseudoscalar $J = 2$ trajectory multiplets, and calculate the pure $s\bar{s}$ mass for the axial-vector $J = 1$ multiplet as well (all masses are given in MeV). We find that these values and the corresponding values in Tables II,IV,VI,VIII are in essential agreement:

Vector: $J = 1$ $M(s\bar{s}) = 1014.5 \pm 0.4$, $J = 3$ $M(s\bar{s}) = 1862.3 \pm 9.0$

Tensor: $J = 2$ $M(s\bar{s}) = 1539.4 \pm 5.5$

Pseudoscalar: $J = 2$ $M(s\bar{s}) = 1869.1 \pm 25.3$

Axial-vector: $J = 1$ $M(s\bar{s}) = 1487.9 \pm 30.0$.

Interestingly enough, if one applies the quark model motivated relation mentioned above to calculate the mass of the axial-vector $s\bar{n}$ state using the predicted pure $s\bar{s}$ mass (this work) and the physical $a_1$ (as pure $n\bar{n}$) mass (Ref. [29]) as inputs, one obtains $M(s\bar{n}) = 1359 \pm 25$ MeV, in good agreement with the corresponding value in Table IV.

(ii) *A new $c\bar{u}$ meson, $D(2637)$,* with mass $2637 \pm 2 \pm 6$ MeV, was recently reported by the DELPHI Collaboration [59]. Page [60] has demonstrated from heavy quark symmetry that the width of $D(2637)$ claimed by DELPHI is inconsistent with any bound state with one charm quark predicted in the $D(2637)$ mass region, except possibly $D_3^*$, $D_2$ or $2S$ $D$, among the three $D_2$ being the best candidate. Interestingly enough, the mass of $D_2$ predicted in Table VI, $2692 \pm 19$ MeV, is consistent with the value of the $D(2637)$ mass measured by DELPHI.

(iii) *Our predictions for the mass of the* $B_c$, $B_c^*$ *states* are in a good agreement with the predictions of different models compiled by Kiselev *et al.* [61] which all, including their own prediction, lie in the ranges $6281\pm38$ and $6343\pm26$ MeV, respectively.

The $B_c$ mass that we obtained, $6283\pm79$ MeV, is also consistent with the value $6.40\pm0.39\pm0.13$ reported by the CDF Collaboration [62].

(iv) *The value of the* $B_1$ *meson mass* that we obtained, $5692\pm104$ MeV, is in good agreement with that recently reported from experiment [63]: $5675\pm12\pm4$ MeV.

(v) *States near the trajectory termination point.* As we argued in Secs. II and III, any nonlinear trajectory of the form (5), including the square root, can be expected to fit well the lowest lying states, and discrepancies are likely to arise only for a few states near the trajectory threshold. There are not enough data to confirm or deny this statement, with the possible exception of the $a_2$ trajectory. Our prediction for the mass of $a_6$, which may be the last state on the true $a_2$ trajectory, and is certainly next-to-last on our corresponding square-root trajectory (see discusion in Sec. IV B), is 10% lower than the observed value. This is in contrast to the $a_4$ mass which is lower only by about 1%. The same is true for the $K_4^*$ mass. (Both $a_4$ and $K_4$ lie about 550 MeV below the corresponding thresholds, whereas the observed mass of the $a_6$ is right at our threshold, in contrast to the calculated value which is $\sim200$ MeV below threshold.)

Even though the agreement within the errors is acceptable, in our opinion, this raises the possibility that near the termination point, the true hadron trajectory grows slower than the square-root trajectory. If this possibility is realized, the $K_6^*$ is likely to lie about 10% above the value we predict, and it can be expected to be broad, similar to the observed $a_6$.

It should be mentioned that there are other trajectories for which the second state on the trajectory is known, e.g. some of the vector or pseudoscalar trajectories. There are two factors which prevent observing the possible general tendency of the square-root form to overshoot the true trajectory. First, these states are further away from the threshold than those discussed above, in particular, they are about 770 MeV below threshold for the vector trajectories, and about 1200 MeV for the pseudoscalars. This means that the effect can be expected to be even less than 1%. Second, in both of these cases, we used some of the second states on the trajectories as inputs, thus achieving better agreement with more of the higher mass states on a trajectory.

(vi) *Additivity constraints and mass relations.* Our results for masses are in excellent agreement with available data. This is not suprising, however, because the additivity constraints (26) and (27) are known to lead to high-accuracy higher-power mass relations [64]. Therefore, the numerical spectroscopy results reported here should be viewed solely as a confirmation that the particular square-root form of trajectory does not introduce any systematic biases.

### 3. A consequence of trajectory thresholds

If the hadronic Regge trajectories indeed terminate in $l$, an intriguing possibility that might simplify identification of

states arises. Even though the maximum $l$ is very sensitive to the specifics of the potential (in particular, its long distance behavior) and cannot be determined at all by fitting the bound states, the thresholds turn out to be insensitive to how the potential approaches its asymptotic value and very well determined by the bound state spectra. Recall our numerical simulation of the model in Sec. II: The bound state spectra were well approximated by both extreme cases, the square-root and the logarithmic trajectory. These two forms differ drastically in the maximum $l$ (finite vs infinite), nevertheless, they both predict $T$ within a few percent of the model's true value. We therefore conjecture that one can predict "spectroscopy windows," i.e. ranges of masses for each particular flavor. Even though we cannot obtain stringent error estimates on these predictions, it is conceivable that the deviations from the true values are small.

The most intriguing consequence of this conjecture is, in our opinion, the following: According to our calculations, there are no light quarkonia states beyond about 3.2 GeV. (The highest threshold for light quarkonia is $\sqrt{T_{\eta_s}}=3.10\pm0.11$ GeV.) Even though the charmed states start around 3 GeV, their mixing with glueballs is small. Therefore, if our analysis is right, any state above 3 GeV (to, say, 5 GeV) that does not fit into the charmed spectra can be expected to be predominantly a glueball or an exotic.

### V. SUMMARY AND CONCLUSIONS

Previously [20] we argued that in QCD, the real part of hadronic Regge trajectories should acquire curvature and terminate as a consequence of the flux tube breaking due to pair creation. In this paper, we addressed the issue of what is the specific form of the trajectories. We started with the simple potential model of two heavy quarks in a potential which is screened at large distances, and we have shown that the parent trajectory formed by the bound states of the system can be equally well approximated by the square root and the logarthmic forms. This is not suprising, once the comparison between the potentials which lead to these trajectories, respectively, and the screened potential of the heavy quark model is made. Nevertheless, even though the first two are indistinguishable, the square-root form is closer to the real trajectory because its real part terminates (as does the real part of the heavy quark model), while the logarithmic trajectory grows without bound. This growth is specific to the logarithmic form; any other trajectory of our nonlinear form (5) with $\nu\neq0$ has a termination point. This means that any $\nu\neq0$ would approximate the true trajectory both quantitatively and qualitatively. Different forms can be expected to lead to subtle differences for higher excited states, particularly for those near the threshold. Until a distinction can be made, we choose the square-root trajectory to study real hadronic spectra. A nice feature of this trajectory is that the additivity of inverse slopes reduces to a simple expression which has natural units of mass, and that the parameter $\gamma$ is given simply in units of inverse mass. It is possible that any of these forms, including the square root, grow faster near the threshold than the true trajectory. It is also plausible, although not conclusive, that an indication of this tendency

has been seen in the $a_2$ trajectory. This is also supported by the rate of growth of the lattice potential as compared to the potential which leads to the square-root trajectory, although the lattice potential should not be taken too seriously at large distances.

With the form of trajectory chosen, the parameters need to be fitted. We have typically used masses of few lowest lying states, and/or the intercepts if known and reliable, such as the intercept of the $\rho$ trajectory. We also utilized the additivity requirements. Our calculation is in an excellent agreement with various data, both spectroscopic and scattering, and it is self-consistent (see the discusion of pseudoscalar $b$-mesons).

We conclude that we have provided both strong phenomenological arguments and theoretical considerations which indicate that the hadronic Regge trajectories are essentially nonlinear, and that they can be well approximated by the square-root form (at least for the lowest lying states). This observation has a profound effect on our theoretical understanding of hadronic spectra, namely, it implies that linear confinement is not the single most important factor in determining the position of poles, not even for states as low as the second or third on a trajectory. Perhaps an even more significant consequence of the nonlinearity of trajectories, and, in particular, the existence of the trajectory thresholds, is that it may simplify identification of states in experiments. For example, once the existence of thresholds is established, it would be easier to identify exotic states as those that do not fit in the heavy-quarkonia spectra.

*Note added in proof.* After this paper was sumbitted for publication, we became aware of new measurements of the $B_1$ meson mass: $(5710\pm20)$ MeV by the CDF Collaboration [66], and $(5670\pm10\pm13)$ MeV by the L3 Collaboration [67]. These new values, together with the value that we refer to in the paper, $(5672\pm12\pm4)$ MeV, are consistent with 5690 MeV for the mass of the $B_1$ meson, which is the central value of our prediction in Table VIII.

### APPENDIX A: THE ALLOWED VALUES OF $\nu$

It can be shown that for $n<\nu<n+1$ [for integer $\nu$, $\alpha(t)=\mathrm{Re}\,\alpha(t)$], the trajectory of the form (5) satisfies the following dispersion relation with $n+1$ subtractions:

$$\alpha(t)=\alpha(0)+\alpha'(0)t+\cdots+\frac{\alpha^{(n)}(0)t^n}{n!}$$

$$+\frac{t^{n+1}}{\pi}\int_T^\infty dt'\frac{\mathrm{Im}\alpha(t')}{t'^{n+1}(t'-t)}. \tag{A1}$$

Since for the trajectory (5) $\mathrm{Im}\,\alpha(t)=\sin(\pi\nu)(t-T)^\nu$, the requirement of the positivity of the trajectory imaginary part (this requirement follows from unitarity [25]) leads to $2k<\nu<2k+1$, where $k$ is integer.

For the trajectory parametrization

$$\alpha(t)=-\gamma(-t)^\nu[\log(-t)]^\beta \tag{A2}$$

[which is the $t\gg T$ limit of Eq. (5), up to a power of logarithm] it was shown in [23] that $0\leq\nu\leq1$ and $0<\beta\leq2$.

The range of $\nu$ can be further restricted. The class of dual models called dual amplitudes with Mandelstahm analycity (DAMA) [21] leaves open a corridor for possible asymptotic behavior of $\alpha(t)$, bounded from above by $\sqrt{|t|}$ and from below by $\log(|t|)$ [25]. [DAMA has the Veneziano limit $\alpha(t)\sim t$, but the transition to this limit occurs discontinuously [25].] Thus, in DAMA the range of $\nu$ is squeezed down to $0\leq\nu\leq1/2$.

Hence we consider the value of $\nu$ restricted to lie between 0 and 1/2 [25].

### APPENDIX B: THE DYNAMICS OF THE GENERALIZED STRING MODEL

By varying the action of the generalized string with massive ends (here the dot stands for the derivative with respect to $\tau$, Lorentz invariant evolution parameter for the string),

$$S_{gen}=\int\int d\tau ds L(x,\dot{x},x')+\sum_{i=1,2}L^{(m)}(\dot{x}_i), \tag{B1}$$

one obtains the equations of motion of the generalized string,

$$\frac{d}{d\tau}\frac{\partial L}{\partial\dot{x}}+\frac{d}{ds}\frac{\partial L}{\partial x'}=\frac{\partial L}{\partial x}, \tag{B2}$$

and the boundary conditions which represent the equations of motion of the massive ends:

$$\frac{d}{d\tau}\frac{\partial L^{(m)}}{\partial\dot{x}_i}=\frac{\partial L}{\partial x'}, \quad x=x_i. \tag{B3}$$

In the gauge $\tau=t$ discussed above, the equations of motion of the generalized string reduce to

$$\frac{d}{dt}\frac{\partial L}{\partial\dot{x}}+\frac{d}{ds}\frac{\partial L}{\partial x'}=\frac{\partial L}{\partial x}, \quad x\equiv\mathbf{x}, \tag{B4}$$

and the boundary conditions are

$$m_1\frac{d}{dt}\frac{\dot{x}_1}{\sqrt{1-\dot{x}_1^2}}=\frac{\partial L}{\partial x'}, \quad s=0,$$

$$m_2\frac{d}{dt}\frac{\dot{x}_2}{\sqrt{1-\dot{x}_2^2}}=\frac{\partial L}{\partial x'}, \quad s=\pi. \tag{B5}$$

Let us show that, similarly to the standard case of the string with constant tension, there are solutions to the equations of motion of the generalized string [with the Lagrangian given in Eq. (14)] in the form of a rigid rod connecting the massive ends and rotating with frequency $\omega$ about its center of mass:

$$x(t,s) = \rho(s)(\cos(\omega t), \sin(\omega t), 0). \qquad (B6)$$

Indeed, $\sigma = \sigma(|x|) = \sigma(\rho)$, since $x^2 = \rho^2$; therefore $d\rho/dx = x/\rho = (\cos(\omega t), \sin(\omega t), 0)$, and $d\sigma/dx = d\sigma/d\rho \, d\rho/dx = d\sigma/d\rho \, (\cos(\omega t), \sin(\omega t), 0)$. Hence

$$\frac{\partial L}{\partial x} = \frac{\partial L}{\partial \sigma} \frac{d\sigma}{dx} = -\frac{d\sigma}{d\rho} \rho' \sqrt{1 - \omega^2 \rho^2} (\cos(\omega t), \sin(\omega t), 0).$$
$$(B7)$$

Since also

$$\frac{d}{dt} \frac{\partial L}{\partial \dot{x}} = -\frac{\sigma \omega^2 \rho \rho'}{\sqrt{1 - \omega^2 \rho^2}} (\cos(\omega t), \sin(\omega t), 0), \qquad (B8)$$

$$\frac{d}{ds} \frac{\partial L}{\partial x'} = \left( -\frac{d\sigma}{d\rho} \rho' \sqrt{1 - \omega^2 \rho^2} + \frac{\sigma \omega^2 \rho \rho'}{\sqrt{1 - \omega^2 \rho^2}} \right)$$
$$\times (\cos(\omega t), \sin(\omega t), 0), \qquad (B9)$$

(the last relation is obtained via $d\sigma/ds = d\sigma/d\rho \, \rho'$), it follows that the equations of motion (B4) are satisfied.

One can show that for the rotation (B6), the energy of the generalized string is given by

$$H = \int ds \sqrt{p^2 + \sigma^2 x'^2} = \int ds \frac{\sigma \rho'}{\sqrt{1 - \omega^2 \rho^2}} = \int \frac{d\rho \sigma(\rho)}{\sqrt{1 - \omega^2 \rho^2}}.$$
$$(B10)$$

Similarly, the orbital momentum of the generalized string is

$$J = J_z = \int ds(x p_y - y p_x)$$

$$= \int ds \frac{\sigma \omega \rho^2 \rho'}{\sqrt{1 - \omega^2 \rho^2}} = \int \frac{d\rho \sigma(\rho) \omega \rho^2}{\sqrt{1 - \omega^2 \rho^2}}. \qquad (B11)$$

Interestingly enough, in his book [65] Perkins also presents the above relations for the energy and orbital momentum of the generalized string. He does not however derive these relations from the first principles Lagrangian, as in Eq. (14).

By adding the contribution of the massive ends, one finally has the expressions for the total energy and orbital momentum of the generalized string with massive ends:

$$E = \int_0^{r_1} \frac{d\rho \sigma(\rho)}{\sqrt{1 - \omega^2 \rho^2}} + \int_0^{r_2} \frac{d\rho \sigma(\rho)}{\sqrt{1 - \omega^2 \rho^2}} + \frac{m_1}{\sqrt{1 - \omega^2 r_1^2}}$$

$$+ \frac{m_2}{\sqrt{1 - \omega^2 r_2^2}}, \qquad (B12)$$

$$J = \int_0^{r_1} \frac{d\rho \sigma(\rho) \omega \rho^2}{\sqrt{1 - \omega^2 \rho^2}} + \int_0^{r_2} \frac{d\rho \sigma(\rho) \omega \rho^2}{\sqrt{1 - \omega^2 \rho^2}}$$

$$+ \frac{m_1 \omega r_1^2}{\sqrt{1 - \omega^2 r_1^2}} + \frac{m_2 \omega r_2^2}{\sqrt{1 - \omega^2 r_2^2}}. \qquad (B13)$$

Note that the boundary conditions (B5) define the separations of the massive ends from the center of mass through the following nonlinear equations:

$$\frac{m_i \omega^2 r_i}{\sqrt{1 - \omega^2 r_i^2}} = \sigma(r_i) \sqrt{1 - \omega^2 r_i^2}, \quad i = 1, 2. \qquad (B14)$$

[1] G. Veneziano, Phys. Rep. **9**, 199 (1974).

[2] J.S. Kang and H.J. Schnitzer, Phys. Rev. D **12**, 841 (1975).

[3] B.M. Barbashov and V.V. Nesterenko, *Relativistic String Model in Hadron Physics* (in Russian) (Energoatomizdat, Moscow, 1987).

[4] V.A. Lyubimov, Usp. Fiz. Nauk **123**, 3 (1977) [Sov. Phys. Usp. **20**, 691 (1977)].

[5] UA8 Colloration, A. Brandt *et al.*, Nucl. Phys. **B514**, 3 (1998).

[6] V.N. Bolotov *et al.*, Nucl. Phys. **B73**, 387 (1974).

[7] D. Gross and P. Mende, Phys. Lett. B **197**, 129 (1987); P. Mende, *ibid.* **326**, 216 (1994). (In the latter paper Mende tried to recover the bound in a compact space for certain kinematic configurations. The problem does not disappear in general.)

[8] M.J. Schmidt, Phys. Lett. **43B**, 417 (1973).

[9] P. Fre and L. Sertorio, Nuovo Cimento A **31**, 365 (1976).

[10] L.L. Jenkovszky and A.A. Trushevsky, Nuovo Cimento A **34**, 369 (1976).

[11] R. Dashen, S. Ma, and H.J. Bernstein, Phys. Rev. **187**, 345 (1969).

[12] L.L. Jenkovszky, A.A. Trushevsky, and L. Sertorio, Lett. Nuovo Cimento Soc. Ital. Fis. **15**, 200 (1976).

[13] M. Froissart, Phys. Rev. **123**, 1053 (1961).

[14] L.L. Jenkovszky, Yad. Fiz. **21**, 645 (1975) [Sov. J. Nucl. Phys. **21**, 334 (1975)].

[15] L. Burakovsky and L.P. Horwitz, Nucl. Phys. **A614**, 373 (1997); L. Burakovsky, Phys. Rev. D **58**, 057503 (1998).

[16] S.B. Giddings, F. Hacquebord, and H. Verlinde, Nucl. Phys. **B537**, 260 (1999).

[17] S. Frautschi and B. Margolis, Nuovo Cimento A **56**, 1155 (1968); M. Martinis, *ibid.* **59**, 490 (1969); H. Yabuki, Phys. Rev. **177**, 2209 (1969); K.V. Vasavada, Lett. Nuovo Cimento Soc. Ital. Fis. **2**, 1339 (1971); Phys. Lett. **34B**, a214 (1971); Phys. Rev. D **3**, 2442 (1971).

[18] K.V. Vasavada, Lett. Nuovo Cimento Soc. Ital. Fis. **6**, 453 (1973); ''Phenomenological Regge cuts and square-root trajectories,'' Indiana Univ.-Purdue Univ. Report Print-74-1694 (IUPUI), 1974.

[19] V.N. Gribov, E.M. Levin, and A.A. Migdal, Yad. Fiz. **12**, 173

(1970) [Sov. J. Nucl. Phys. **12**, 93 (1971)].

[20] M.M. Brisudová, L. Burakovsky, and T. Goldman, Phys. Lett. B **460**, 1 (1999).

[21] A.I. Bugrij, G. Cohen-Tannoudji, L.L. Jenkovszky, and N.I. Kobylinsky, Fortschr. Phys. **11**, 427 (1973).

[22] K.D. Born *et al.*, Phys. Rev. D **40**, 1653 (1989).

[23] A.A. Trushevsky, Ukr. Fiz. Zh. (Russ. Ed.) **22**, 353 (1977).

[24] D. Crewther and G.C. Joshi, Phys. Rev. D **9**, 1446 (1974).

[25] L.L. Jenkovszky, Riv. Nuovo Cimento **10**, 1 (1987).

[26] N.A. Chernikov and N.S. Shavokhina, Theor. Math. Phys. **42**, 38 (1980); N.S. Shavokhina, Sov. Phys. J. **7**, 641 (1983); **12**, 1104 (1984).

[27] L. Burakovsky (in preparation).

[28] L. Burakovsky and T. Goldman, Phys. Lett. B **434**, 251 (1998).

[29] Particle Data Group, C. Caso *et al.*, Eur. Phys. J. C **3**, 1 (1998).

[30] R.K. Logan and L. Sertorio, Phys. Rev. Lett. **17**, 834 (1966).

[31] F. Arbab and C.B. Chiu, Phys. Rev. **147**, 1045 (1966).

[32] V.N. Bolotov *et al.*, Nucl. Phys. **B73**, 365 (1974).

[33] V. Barger, plenary session talk at the XVII International Conference on High Energy Physics, London, 1974.

[34] G. Höhler, J. Baacke, H. Schlaile, and P. Sonderegger, Phys. Lett. **20**, 79 (1966); G. Höhler, J. Baacke, and J. Eisenbeiss, *ibid.* **22**, 203 (1966); G. Höhler, H.P. Jakob, and P. Kroll, Z. Phys. **261**, 401 (1973).

[35] G. Höhler and H.P. Jakob, ''Tables of pion-nucleon forward amplitudes,'' Univ. of Karlsruhe Report TKP 23/72 (1972).

[36] R.E. Hendrick *et al.*, Phys. Rev. D **11**, 536 (1975).

[37] A.S. Carroll *et al.*, Phys. Lett. **61B**, 303 (1976).

[38] A. Bouquet, Z. Phys. C **3**, 65 (1979).

[39] A. Donnachie and P.V. Landshoff, Phys. Lett. B **296**, 227 (1992).

[40] N.A. Kobylinsky and V.V. Timokhin, Ukr. Fiz. Zh. (Russ. Ed.) **24**, 1142 (1979).

[41] N.A. Kobylinsky and A.B. Prognimak, Acta Phys. Pol. B **9**, 149 (1978).

[42] V.B. Vinogradov, N.A. Kobylinsky, Yu.A. Kulchitsky, and V.V. Timokhin, Yad. Fiz. **44**, 212 (1986) [Sov. J. Nucl. Phys. **44**, 134 (1986)] and references therein.

[43] VES Collaboration, D.V. Amelin *et al.*, hep-ex/9810013.

[44] VES Collaboration, V. Dorofeev *et al.*, hep-ex/9905002.

[45] NRQCD Collaboration, C.T.H. Davies *et al.*, Nucl. Phys. B (Proc. Suppl.) **60**, 124 (1998); **63**, 320 (1998).

[46] L. Burakovsky and T. Goldman, Nucl. Phys. **A625**, 220 (1997).

[47] J.-R. Cudell, K. Kang, and S.K. Kim, Phys. Lett. B **395**, 311 (1997); hep-ph/9701312; hep-ph/9812429.

[48] I.G. Alekseev *et al.*, Yad. Fiz. **61**, 223 (1998) [Phys. At. Nucl. **61**, 174 (1998)].

[49] A.G. Oganesyan and A.Yu. Khodzhamiryan, Yad. Fiz. **56**, 172 (1993) [Phys. At. Nucl. **56**, 1720 (1993)].

[50] A.H. Muller, Phys. Rev. D **2**, 2963 (1970).

[51] LEBC-EHS Collaboration, M. Aguilar-Benitez *et al.*, Phys. Lett. **161B**, 400 (1985).

[52] WA75 Collaboration, S. Aoki *et al.*, Phys. Lett. B **209**, 113 (1988); Prog. Theor. Phys. **87**, 1315 (1992).

[53] ACCMOR Colloration, S. Barlag *et al.*, Phys. Lett. B **247**, 113 (1990); Z. Phys. C **49**, 555 (1991).

[54] WA82 Collaboration, M.I. Adamovich *et al.*, Nucl. Phys. B (Proc. Suppl.) **27**, 212 (1992); Phys. Lett. B **305**, 402 (1993).

[55] E769 Collaboration, G.A. Alves *et al.*, Phys. Rev. Lett. **69**, 3147 (1992); **70**, 722 (1993); **72**, 812 (1994); **77**, 2388 (1996); **77**, 2392 (1996).

[56] E769 Collaboration, G.A. Alves *et al.*, Phys. Rev. D **49**, R4317 (1994).

[57] Fermilab E515 Collaboration, M. Sarmiento *et al.*, Phys. Rev. D **45**, 2244 (1992).

[58] L. Burakovsky, P.R. Page, and T. Goldman, Phys. Lett. B **467**, 255 (1999).

[59] DELPHI Collaboration, P. Abreu *et al.*, Phys. Lett. B **426**, 231 (1998).

[60] P.R. Page, Phys. Rev. D **60**, 057501 (1999).

[61] V.V. Kiselev, A.K. Likhoded, and A.V. Tkabladze, Yad. Fiz. **58**, 1045 (1995) [Phys. At. Nucl. **58**, 972 (1995)]; S.S. Gershtein, V.V. Kiselev, A.K. Likhoded, and A.V. Tkabladze, Phys. Rev. D **51**, 3613 (1995).

[62] CDF Collaboration, F. Abe *et al.*, Phys. Rev. Lett. **81**, 2432 (1998); Phys. Rev. D **58**, 112004 (1998).

[63] F. Muheim, hep-ex/9902026, and references therein.

[64] L. Burakovsky, T. Goldman, and L.P. Horwitz, Phys. Rev. D **56**, 7119 (1997); **56**, 7124 (1997); J. Phys. G **24**, 771 (1998).

[65] D.H. Perkins, *Introduction to High Energy Physics*, 3rd ed. (Addison-Wesley, Menlo Park, CA, 1987), Sec. 8.10.

[66] CDF Collaboration, G. Bauer, hep-ex/9909014.

[67] L3 Collaboration, L3 Note 2423, 1999.